Journal of Marine Research, 54, 407–420, 1996

Journal of
MARINE RESEARCH

Volume 54, Number 3

Grid-scale instability of convective-adjustment schemes

by Paola Cessi[1,2]

ABSTRACT

Through a simple illustrative example, it is shown that instantaneous convective adjustment schemes, of the type used in general circulation models to parametrize nonhydrostatic convective processes, lead to the spontaneous emergence of the smallest resolved horizontal scale: the grid mode is unstable regardless of the strength of the horizontal diffusivity. Convective adjustment vertically mixes properties at each grid-point, irrespective of the horizontal distribution of such properties. Thus, horizontal spatial gradients are amplified by convective adjustment, as long as adjustment is faster than the horizontal diffusion (or advection) time between neighboring grid-points. In the example presented here, the grid-scale instability is a global attractor and can only be "suppressed" by inaccurate time-stepping, or by the finite computational representation of numbers. This clarifies that the "grid-mode" is not a computational instability, but an intrinsic property of instantaneous convective adjustment schemes. A smooth solution, without grid-scale gradients, also exists, but it is unstable to infinitesimal perturbations for *all* values of the external parameters. We emphasize that the spatial average of the grid-mode differs substantially from the spatial average of the smooth (but unstable) solution.

1. Introduction

In general circulation models of the oceans, static instabilities (heavy fluid over light) are removed by "convective adjustment" (CA) algorithms. The essential idea is that when unstable stratification is detected in a column of fluid, temperature and salinity are rapidly mixed vertically to produce a neutrally stable state (Bryan, 1969). There are different implementations of CA algorithms (e.g., Marotzke, 1991; Yin

1. Scripps Institution of Oceanography, La Jolla, California, 92093-0230, U.S.A.
2. Istituto FISBAT-CNR, I-40129 Bologna, Italy.

and Sarachik, 1994), but a common aspect is that the decision to adjust is based on vertical density gradients and ignores *horizontal* differences in density. Therefore, if CA occurs at one grid-point, but not at a neighboring one, then a density gradient on the grid-scale is created very rapidly.

This obvious deficency of CA algorithms has not undermined their popularity because of the widespread conviction that advective-diffusive processes can destroy grid-scale gradients, and that, in any case, the average properties are unchanged by a grid-scale modulation.

There is ample evidence in both the oceanographic literature (Rahmstorf and Willebrand, 1995) and in day-to-day practice (Meacham, personal communication) that advective-diffusive processes are not guaranteed to suppress instability at the smallest resolved scale. Indeed, the emergence of grid-scale patterns is a plague not limited to ocean general circulation models (GCM's); atmospheric models using moist convective adjustment exhibit precipitation on the grid-scale (e.g., Numaguti and Hayashi, 1991). In all the cited examples the origin of the grid-scale structure is unclear because of the complexity of motions that can be excited: small-scale gravity waves have been considered a prime suspect for the generation of small-scale structure in the tropical atmosphere (Lindzen, 1974). Moreover, in a GCM it is not possible to test whether the grid-scale modulation alters the spatially averaged properties of the fields of interest.

Here we illustrate, through a minimal example, that gradients on the grid-scale are excited solely by convective adjustment in a horizontally extended system. Further, the spatially averaged fields are very different depending on whether the grid-mode is allowed or suppressed. These results stress the necessity of developing parametrizations of convective processes that are stable and correctly describe the physics of sub-grid scales.

2. Formulation

Consider a well-mixed layer of fluid, overlying an infinitely deep layer, where the density, ρ, depends linearly on the temperature, T, and the salinity, S, i.e. $\rho = S - T$. (cf. Fig. 1). For simplicity we assume that the temperature of the upper layer is kept fixed to the value $T(x, t) = 1$, and both the temperature and salinity of the lower layer are kept at reservoir values: $S_0(x, t) = T_0(x, t) = 0$. The salinity of the top layer is continuously increased by a specified flux, of unit magnitude, and it is allowed to diffuse laterally downgradient. Whenever the density of the top layer exceeds that of the lower layer, the static instability is removed instantaneously, by mixing the salinity vertically, and thus setting $S(x, t)$ equal to the reservoir value. This rapid mixing is the convective-adjustment rule. Thus the model is:

$$\begin{aligned} \partial_t S &= 1 + \alpha \partial_x^2 S, \qquad \text{if } S \leq 1 \\ S &\to 0, \qquad\qquad\quad \text{if } S > 1, \end{aligned} \tag{2.1a,b}$$

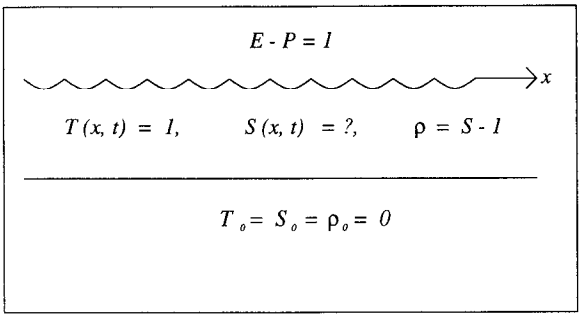

Figure 1. A schematic drawing of the diffusively coupled thermohaline oscillators. A layer of vertically homogeneous fluid of density $\rho = S(x, t) - T(x, t)$ is below an "atmosphere" providing a constant evaporation-precipitation flux of unit magnitude. In this layer the temperature is maintained at the constant value, $T = 1$, while the salinity evolves in time and space due to the E-P flux, horizontal downgradient diffusion and convective adjustment. The temperature and salinity of the deep reservoir are maintained to the value $T_0 = S_0 = 0$. Whenever the density of the top layer exceeds that of the deep reservoir convective adjustment occurs, i.e. the top salinity is instantaneously mixed to the reservoir value.

where $0 \leq x \leq 1$. We avoid end-effects by considering a periodic system with $S(x, t) = S(x + 1, t)$.

Notice that the temperature of the upper layer is fixed to the value 1, while the salinity evolves in time: we are considering a scenario in which the thermal relaxation is much more rapid than that of salinity (Stommel, 1961; Bryan, 1986). This is the fundamental asymmetry between heat and salt in the system.

For expository purposes we have used the case of salinity-driven "convection." Other configurations, after suitable rescaling, can be put in a form resembling (2.1). In (2.1a) weak vertical mixing with the deep lower layer that might occur in stably stratified conditions has been neglected (this would amount to adding $-kS$ to the right-hand side of (2.1a)). This generalization has been explored and it has no qualitative impact on the conclusions. Finally, we have assumed that the forcing is spatially uniform: we find that the system spontaneously generates spatially modulated salinity fields. In our opinion it is important to understand these intrinsic sources of spatial variability before examining the interaction with externally imposed spatial nonuniformities.

The formulation (2.1), because of the adjustment rule, must be interpreted in the context of a discretized model. As it stands, $\partial_x^2 S$ is not defined after the CA rule has been applied. Or perhaps it is not clear how convective adjustment can be implemented in a continuous (or even a spectral) model. This shortcoming applies equally to all GCMs that use CA. However the difficulty with the continuous limit is not an objection to the modeling strategy, as long as the model is interpreted as a set of coupled ordinary differential equations (in time), obtained by spatially discretizing the continuous system. Specifically, we divide the domain $0 \leq x \leq 1$ into N intervals

of length $h \equiv 1/N$ so that $x = nh$, and $1 \leq n \leq N$. The state of the system at time t is defined by the vector with components $S_n(t)$ which evolves according to

$$\begin{aligned} S_n &= 1 + \alpha N^2(S_{n+1} - 2S_n + S_{n-1}), && \text{if } S_n \leq 1, \\ S_n &\to 0, && \text{if } S_n > 1. \end{aligned} \tag{2.2a,b}$$

Although, for numerical implementation, the system (2.2a) must also be discretized in time, we consider time to be continuous. In the next section, analytic solutions of (2.2) are discussed, and this provides some assurance that the semi-discrete formulation above in (2.2) is well posed.

3. The homogeneous solution and its stability

The system (2.2) has a simple solution in which all the S_n's are equal

$$S_n(t) = t - \text{int}(t), \tag{3.1}$$

where int(t) is the integer part of t, e.g. int(π) = 3 and int(e) = 2. In this spatially uniform solution all the grid-points are adjusting in synchrony at $t = 1, 2, 3, \ldots$. This solution is analogous to the thermohaline relaxation-oscillations isolated by Welander (1982). However, with many thermohaline oscillators coupled diffusively, the spatially uniform solution is unstable to disturbances on the grid-scale.

Figure 2 shows the space-time coordinates of CA events for a numerical integration of (2.2) using the simplest time-discretization scheme: forward Euler. Specifically, given the present state $S_n(t)$, we define the tentative future state by:

$$\hat{S}_n(t + dt) \equiv S_n(t) + dt + dt(\alpha N^2)\,[S_{n+1}(t) - 2S_n(t) + S_{n-1}(t)], \tag{3.2}$$

where dt is the time step. We then apply CA and obtain the true future state by using the rule:

$$\begin{aligned} S_n(t + dt) &= \hat{S}_n(t + dt) && \text{if } \hat{S}_n(t + dt) \leq 1, \\ S_n(t + dt) &= 0 && \text{if } \hat{S}_n(t + dt) > 1. \end{aligned} \tag{3.3a,b}$$

In the computation of Figure 2 the initial condition, $S_n(0)$, is a random number between 0 and 0.01 picked from a uniform distribution. The first CA events are at about $t = 1$, as expected from the simple spatially uniform solution (3.1), but they occur at every other grid-point (except for four "defects" located at $n = 5, 16, 65, 92$). Notice that the decay time for the mode alternating in space at every grid-point, i.e., $S_n(t) = a(t)(-1)^n$, is $(4\alpha N^2)^{-1}$. For the computation shown, with $\alpha = 0.0003$ and $N = 100$, the decay time of a grid-mode is 1/12, and yet CA is still occurring on the grid-scale at $t = 20$. Consequently, the salinity field at the final time, shown in Figure 3, has a "noisy" spatial distribution, with structure down to the smallest resolved scale. The spatially uniform solution in (3.1) is apparently never reached from the initial condition used in Figure 2.

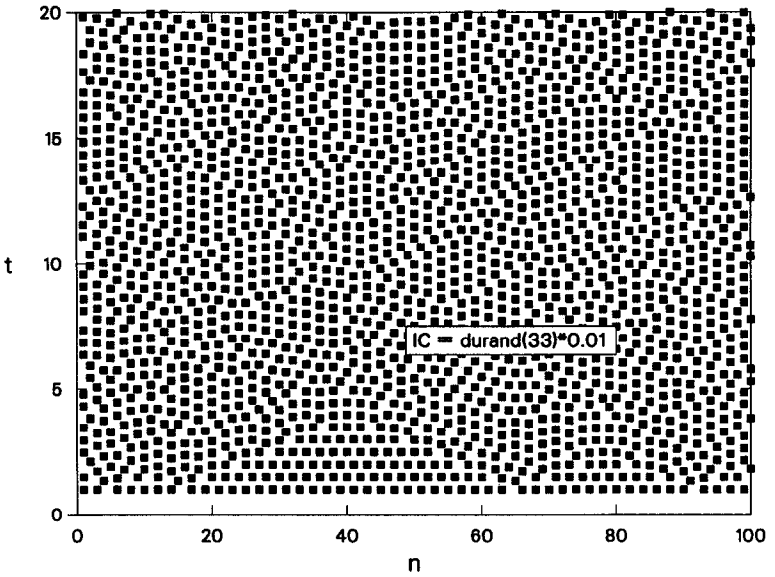

Figure 2. The space-time coordinates of convective adjustment events for a numerical integration of the system (3.2) − (3.3) with $\alpha = 0.0003$, $N = 100$, $dt = 1/(128N^2)$. The initial condition $S_n(0)$ is a random number between 0 and 0.01 picked from a uniform distribution (we used the ESSL subroutine DURAND with seed = 33). All the variables in the computation are in double precision.

In the following we present evidence that the spatially uniform solution is unstable to infinitesimal disturbances on the grid-scale, for *all* values of αN^2, i.e. the grid-mode is unstable no matter how fine the spatial resolution and no matter how large the horizontal diffusion.

4. The return map for the grid-mode

Let us look for a particular solution of (2.2) such that the values of S at all the even grid-points are equal, and those at all the odd ones are equal:

$$\begin{aligned} S_{2n}(t) &= a(t), \\ S_{2n+1}(t) &= b(t). \end{aligned} \tag{4.1}$$

Then, the system of N coupled equations in (2.2) is reduced to the pair

$$\begin{aligned} \dot{a} &= 1 + \beta(b - a)/2 \qquad \text{if } a \leq 1, \\ a &\to 0 \qquad\qquad\qquad\quad \text{if } a > 1, \\ \dot{b} &= 1 + \beta(a - b)/2 \qquad \text{if } b \leq 1, \\ b &\to 0 \qquad\qquad\qquad\quad \text{if } b > 1, \end{aligned} \tag{4.2a,b,c,d}$$

where $\beta \equiv 4\alpha N^2$. We assume that at $t = 0$ a has just undergone CA and $b(0) = B$.

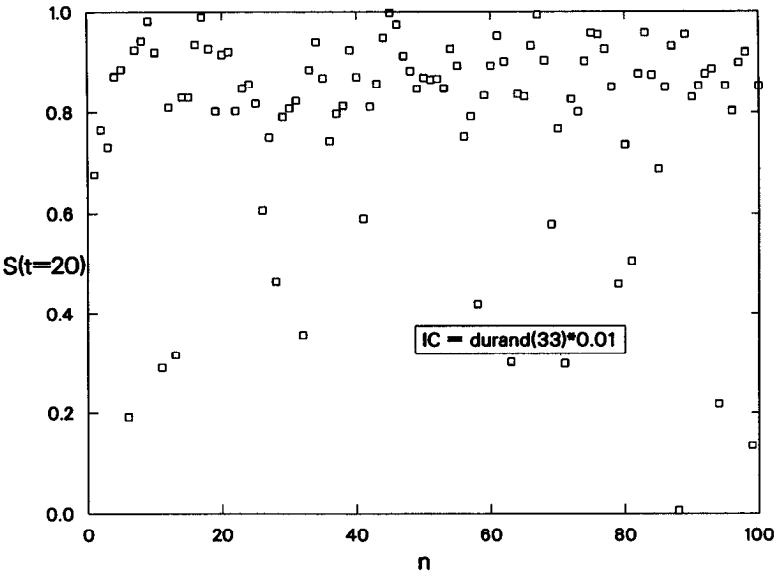

Figure 3. The salinity as a function of the space-coordinate n at the final time of the computation described in Figure 2, S_n (20). We resisted the temptation to connect the points in order to emphasize that there is structure down to the smallest resolved scale.

After any adjustment, a and b have values only between 0 and 1, so we may consider B to be positive. Until the next CA event, the solution of (4.2) is

$$\begin{aligned} a(t) &= t + B[1 - \exp(-\beta t)]/2, \\ b(t) &= t + B[1 + \exp(-\beta t)]/2. \end{aligned} \tag{4.3}$$

In this case b will reach the threshold for CA before a, at the time $t = \tau_1$, given by the solution of the transcendental equation,

$$\tau_1 = 1 - B[1 + \exp(-\beta\tau_1)]/2. \tag{4.4}$$

An example of the phase plane, (a, b), is shown in Figure 4 for $\beta = 2.25$. At $t = \tau_1$, a will be

$$a(\tau_1) = 2\tau_1 + B - 1. \tag{4.5}$$

After this first adjustment, the roles of a and b are exchanged. Now it will be a that adjusts next, at the time $t = \tau_1 + \tau_2$, with τ_2 satisfying:

$$\tau_2 = 1 - a(\tau_1)[1 + \exp(-\beta\tau_2)]/2. \tag{4.6}$$

At $t = \tau_1 + \tau_2$, b will be

$$b(\tau_1 + \tau_2) = 2\tau_2 + a(\tau_1) - 1. \tag{4.7}$$

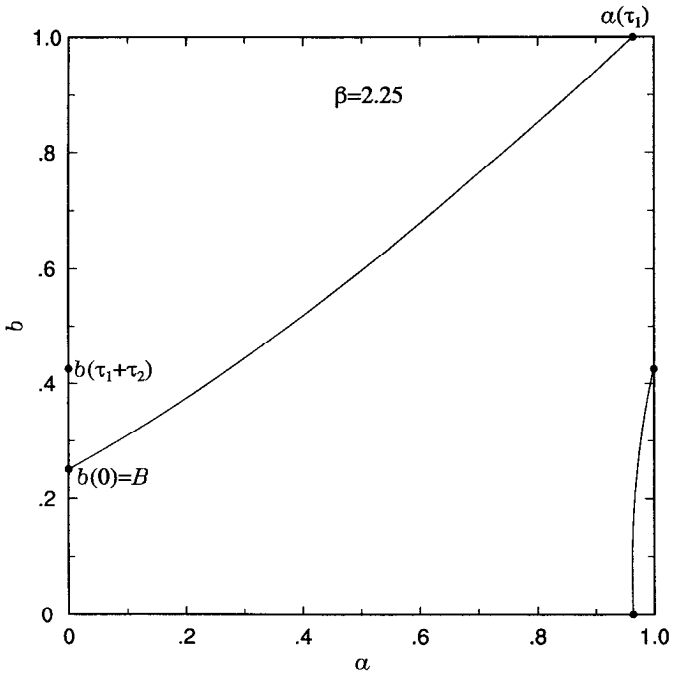

Figure 4. The phase plane (a, b), solutions of (4.2). At $t = 0$, a has just adjusted and $b(0) = B$. At $t = \tau_1$ the system reaches the point $(a(\tau_1), 1)$ and at this instant b adjusts, bringing the system to $(a(\tau_1), 0)$. Next, at $t = \tau_1 + \tau_2$, a adjusts and the system reaches $(0, b(\tau_1 + \tau_2))$. The return map is obtained by calculating $b(\tau_1 + \tau_2)$ as a function of $b(0)$.

Thus, given B_i, the value of b at the time of a CA for a, we can find B_{i+1}, the value of b at the next a adjustment, by solving the set of nonlinear transcendental equations:

$$B_{i+1} = F(F(B_i)),$$
$$F(B) = 2\tau(B) + B - 1, \qquad (4.8a,b,c)$$
$$\tau(B) = 1 - B\{1 + \exp[-\beta\tau(B)]\}/2.$$

Here $\tau(B_i)$ is τ_1 in (4.4), i.e. the time for b to reach the CA threshold. $F(B_i)$ is equal to $a(\tau_1)$ in (4.5) and τ_2 in (4.6) is identified with $\tau(F(B_i))$. The final value, $b(\tau_1 + \tau_2)$ in (4.7), at the end of the adjustment cycle is B_{i+1}. The procedure (4.8) requires the numerical solution of a simple transcendental equation for $\tau(B)$. The mapping in (4.8) can be iterated many times to obtain successive values of B_i. If any B_i is zero or larger than one, then the even and odd grid-points adjust simultaneously and the spatially homogeneous solution (3.1) emerges. Because the algorithm in (4.8) only gives the values of $b(t)$ at the times when $a(t)$ goes through CA we call it a return map.

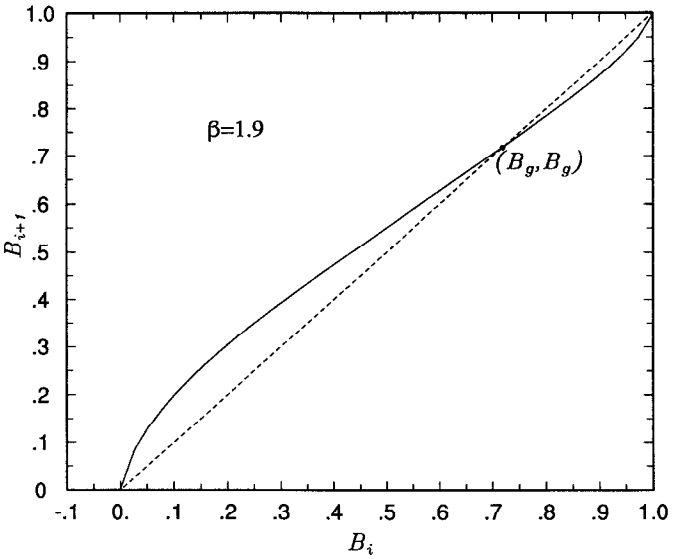

Figure 5. The return map of the grid-mode showing, B_{i+1}, the solution of (4.8), as a function of B_i, for $\beta = 1.9$ (solid line). The dashed line is the identity map $B_{i+1} = B_i$. If the odd grid-points start at the value B_i at the time when the even grid-points are adjusting, they will be at B_{i+1} at the next CA event of the even grid-points. The intersections of the return map with the identity map are periodic solutions in time. If the slope of the return map at these intersections exceeds one, then they are unstable. If the slope is less than one, then the fixed point is stable. The origin, corresponding to the spatially homogeneous solution (3.1), is unstable for all values of the coupling coefficient β.

One way to visualize concisely the results of applying the algorithm (4.8) is to plot B_{i+1} as a function of B_i, with $0 \leq B_i \leq 1$ for different values of the coupling coefficients β. A graph of $F(F(B_i))$ versus B_i, for $\beta = 1.9$, is shown in Figure 5. Given an initial condition B_i, the long-time evolution of the system (4.2) can be inferred graphically using the return map. Points where the curve of $F(F(B_i))$ intersects the line $B_{i+1} = B_i$, correspond to periodic solutions of the system (4.2), because when a comes back to the same value (0 in this case), b also returns to the value it started from. If the slope of the return map is less than unity at these intersection points, the periodic solution is stable, and if the slope is larger than unity, then the periodic solution is unstable (Berge *et al.*, 1986).

The return map in Figure 5 shows that the spatially homogeneous solution, corresponding to the point $(B_i, B_{i+1}) = (0, 0)$ or $(B_i, B_{i+1}) = (1,1)$, is unstable to infinitesimal perturbations. But there is another globally attracting limit cycle with $B_i = B_{i+1} = B_g$. This attractor is a fixed point of (4.8):

$$\tau(B_g) = \tau(F(B_g)) = \tfrac{1}{2},$$
$$B_g = F(B_g) = F(F(B_g)) = [1 + \exp(-\beta/2)]^{-1}. \qquad (4.9a,b)$$

The fixed point in (4.9) corresponds to a state where all the odd grid-points (i.e. the b's) are at a finite value, given by (4.9b) when all the even grid-points (i.e. the a's) are adjusting. Conversely, at the times when the odd grid-points are adjusting, the even grid-points are at $F(B_g)$ in (4.9b). The time to go through one of these half-cycles is precisely $\tau = \frac{1}{2}$, so that the period of the grid-mode is 1, the same as the spatially homogeneous (but unstable) solution (3.1). However the spatially averaged salinity of the grid-mode, $\overline{S_g}(t) \equiv (a + b)/2$, is different from the spatially averaged salinity of the homogeneous solution (which is obtained if one starts exactly at $b(0) = 0$). For the grid-mode

$$\overline{S_g}(t) = t - \text{int}(2t)/2 + B_g/2, \tag{4.10}$$

so that the time and space averaged salinity is

$$\int_0^1 \overline{S_g}(t)\, dt = \frac{1}{4} + B_g/2. \tag{4.11}$$

The time-average of the spatially homogeneous solution, (3.1), is simply $\frac{1}{2}$, as is (4.11) in the limit of $\beta \to 0$, i.e. in the weakly coupled limit. Conversely, in the strongly diffusive limit, $\beta \to \infty$, the time and space average of the grid-mode salinity approaches $\frac{3}{4}$. Counterintuitively, when the coupling between neighboring grid-points is large the macroscopic properties of the grid-mode differ the most from those of the spatially homogeneous solution.

In fact, the instability of the spatially homogeneous solution, measured by the slope of the return map minus unity at the origin, increases as β increases and for $\beta > 2$ the return map (4.8) is discontinuous at the point $B_i = 0$. Figure 6 shows the solutions of the return map (4.8) for $\beta = 3$. For $\beta > 2$, a qualitative change occurs in $F(F(B_i))$ (cf. Fig. 5 with Fig. 6): the return map is everywhere concave, still intersecting the point (B_g, B_g) with a slope less than unity. To understand this point it is useful to examine the behavior of the solutions to (4.8) when $B_i \to 0$. In this limit, the time for the first adjustment of b is $\tau(B_i)$ in (4.8c) and is given by

$$\tau(B_i) = 1 - B_i[1 + \exp(-\beta)]/2 + O(B_i^2). \tag{4.12}$$

Because b starts very close to zero, when it reaches the CA threshold, $a(\tau(B_i))$ is very close to one and it is given by

$$F(B_i) = 1 - B_i[1 + \exp(-\beta)] + O(B_i^2). \tag{4.13}$$

Intuitively one would assume that because $F(B_i)$ is close to one, the time, τ_2, taken by a to reach the CA threshold is very short. However, this is not the case when $\beta > 2$. This time is given by the implicit relation

$$\tau_2 = 1 - F(B_i)[1 + \exp(-\beta\tau_2)]/2. \tag{4.14}$$

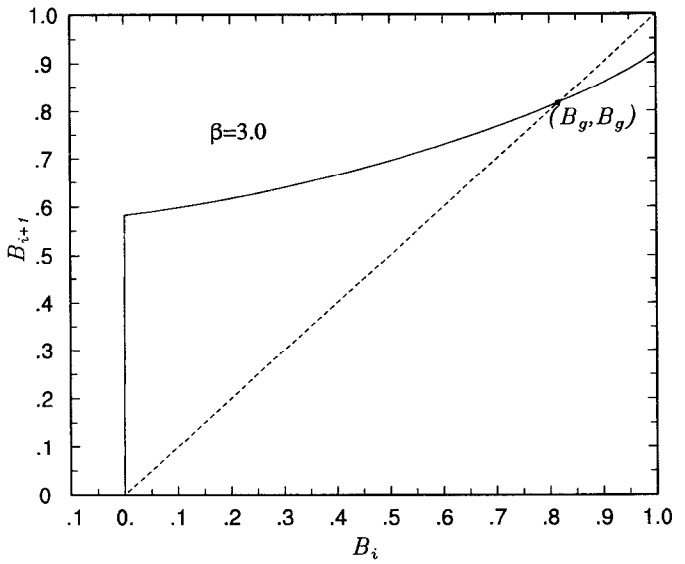

Figure 6. Same as Figure 5, except that $\beta = 3$. Now the return map is discontinuous at the origin, which is still unstable. For values of $\beta \leq 2$ the return map is qualitatively similar to that of Figure 5. For $\beta > 2$, the return map is similar to that of Figure 6. In all cases there is a globally attracting limit cycle such that the even and odd grid-points exchange their value periodically. At any given time, the salinity, S_n oscillates in space with wavelength $n = 2$.

This equation can be solved graphically by plotting $F(B_i)$ as a function of τ_2

$$F(B_i) = 2(1 - \tau_2)[1 + \exp(-\beta\tau_2)]^{-1}, \tag{4.15}$$

as shown in Figure 7 for three values of β: 1, 2 and 3. For all values of β, $F(B_i)$ is equal to one at $\tau_2 = 0$ and for $\beta < 2$ it is a monotonic decreasing function of τ_2. However, for $\beta > 2$, $F(B_i)$ first increases to a value larger than one and then decreases after reaching a maximum, so that the intersection of the curve (4.15) with (4.13) occurs for τ_2 of order one, even if $F(B_i)$ is infinitesimally smaller than unity. In summary, the spatially homogeneous solution in (3.1) is unstable to the grid-mode for all values of the coupling coefficient $\beta \equiv 4\alpha N^2$.

5. Numerical suppression of the grid-mode

The conclusion in the previous section applies to the semi-discrete system in (2.2) and it must be qualified when discussing the fully discrete implementation of (2.2) on a computer. The fully discrete system is defined by (3.2) and (3.3). In the course of applying the test in (3.3) there may be a subtraction of two numbers which are equal to within machine precision. The roundoff error will result in the "numerical suppression" of the grid mode. This numerical suppression occurs most easily when β is very large.

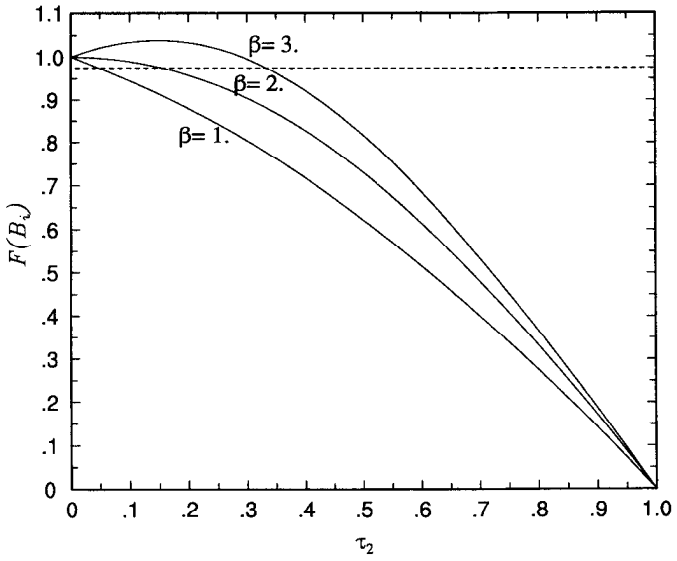

Figure 7. A graph of $F(B_i)$ in (4.15) as a function of τ_2 for three different values of the coupling coefficient β (solid line). The dashed line is the constant $F(B_i) = 0.975$. $F(B_i)$ is the value of the even grid-points at the time of the first CA for the odd grid-points initially at B_i. τ_2 is the time it takes the even grid-points to reach the CA threshold. The intersection between the solid and dashed line gives τ_2. This graph illustrates the change in qualitative behavior as β goes through 2. For $\beta \leq 2$, τ_2 is a continuous function of $F(B_i)$. For $\beta > 2$, τ_2 is discontinuous at $F(B_i) = 1$.

When $\beta \gg 1$ the value of b after one full cycle is

$$B_{i+1} = 1 - e^{-\beta/2} - \beta e^{-\beta}/2 + B_i(1 + \beta/2)e^{-\beta(3-B_i)/2} + O\,(e^{-\beta(2-B_i/2)}). \qquad (5.1)$$

In (5.1), the difference between B_{i+1} and 1 is $O[\exp(-\beta/2)]$, which becomes very small when β becomes large. In a time-stepping code the error in calculating the distance of $S_n(t)$ from the CA threshold is of the order of the time-step. This error might easily exceed $\exp(-\beta/2)$ when N is large (recall that $\beta = 4\alpha N^2$). When an error brings B_{i+1} above 1, the odd and even grid-points adjust simultaneously, $a = b$, and the uniform solution (3.1) is obtained. Figure 8 shows two time-series of $a(t) - b(t)$, obtained by solving (4.2), with $\beta = 12$, using the same scheme as (3.2) and (3.3) (Euler forward) but two different time-steps. The dashed line shows a computation with $dt = [\exp(-\beta/2)]/2$ and in this case the grid-mode is accurately captured. The solid line shows a computation with $dt = 2\exp(-\beta/2)$ and in this case the grid-mode is suppressed, eventually $a(t) = b(t)$ and the uniform solution (3.1) is obtained. Notice that the time-step for the "inaccurate" solution in Figure 8 (solid line) satisfies the criterion for computational stability

$$\exp(-\beta/2) < dt < \beta^{-1}, \qquad (5.2)$$

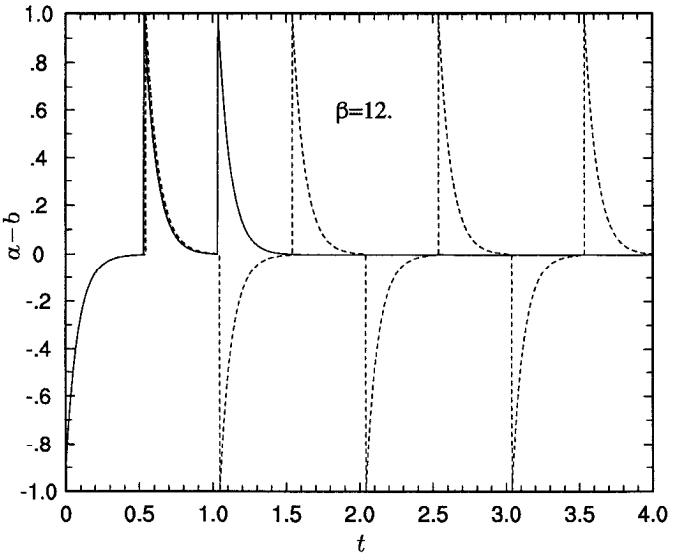

Figure 8. Two time series of the difference $a(t) - b(t)$, obtained by solving (4.2) numerically, using the scheme defined in (3.2) and (3.3), i.e. the grid-points are all advanced in time with Euler forward, and then tested for static stability. The integration shown with the dashed-line used a time step $dt = [\exp(-\beta/2)]/2$, which accurately captures the grid-mode. The solid line shows an integration with $dt = 2\exp(-\beta/2)$: with this larger time-step the grid-mode is suppressed and the uniform solution (3.1) is obtained.

but it is not small enough to resolve the exponentially small correction in (5.1) which prevents the emergence of the uniform solution and establishes the grid-mode. As mentioned earlier roundoff errors, due to the finite representation of numbers in computations can also lead to spatial homogenization. If the machine precision is ϵ, then homogenization occurs for

$$\epsilon > \exp(-\beta/2). \tag{5.3}$$

For example, using double-precision variables, ϵ is of order 10^{-16} and "homogenization" occurs for $\alpha N^2 \gtrsim 35$.

The preceding discussion emphasizes the distinction between an algorithm and its numerical implementation. We have shown that an accurate numerical implementation of CA leads to a grid-scale instability. The generation of structure on the smallest resolved spatial scale is an undesirable feature of convective adjustment. It is ironic that an inaccurate numerical representation of the CA algorithm can result in the suppression of the grid-mode.

6. Discussion

The reason why, at least in principle, the grid-mode emerges regardless of the grid-size, $h \equiv 1/N$, and the diffusive coupling, α, is clear. Even if two neighboring

grid-points are both very close to the CA threshold, as long as one of them reaches it before the other, a large gradient will be generated instantaneously. Thus we conjecture that this generation mechanism of grid-scale gradients operates also in models more complex than the one examined here. Specifically, the grid-mode formulation (4.2) applies exactly in two additional cases:

(1) When advection by a constant velocity, U, is added in (2.2) using upstream differencing for the advection term, (4.2) still holds with a different definition of the constant β (β is now given by $4\alpha N^2 + 2|U|N$).

(2) If (2.2) is generalized to two dimensions (with isotropic diffusivities), then (4.2) is obtained when considering a and b to be the values of the salinity S at alternating grid-points in a regular checker-board pattern.

Presumably, if the duration of CA were finite, say τ_{CA}, gradients could be sustained against diffusion on a scale larger than $l_{CA} = O(\sqrt{\alpha\tau_{CA}})$; however the physical significance of l_{CA} is obscure. A finite duration of convective adjustment is used in implicit schemes that enhance the vertical diffusion when unstable density stratification is detected (Cox, 1984).

In our opinion, the grid-mode is an unwanted artifact of the instantaneous CA procedure. We have shown that it can be suppressed by a combination of finite time-step, dt, and roundoff error, ϵ. Because this grid-scale modulation is the result of the CA algorithm and not a computational mode, it is when dt and ϵ are sufficiently *large* that the grid mode is suppressed. In any event, it is unfortunate that dt and ϵ acquire the status of adjustable parameters.

The presence of the grid-mode is important because it has a large scale, averaged salinity very different from that of the spatially uniform solution. It is possible that the spatially uniform solution (3.1) is unstable to other grid-scale perturbations, each with its own spatially averaged salinity distribution. Thus suppression of the grid-scale instabilities and the development of parametrizations of convective processes that are grid-mode free and correctly capture the effect of unresolved scales is not merely an aesthetic issue.

Acknowledgments. Numerous conversations with Bill Young, Maurizio Fantini and Piero Malguzzi are gratefully acknowledged. Funding for this research is provided by the Department of Energy through its CHAMMP Program (DOE DEFG03 93ER61690) and by the Commission of the European Communities through its MAST II Programme (MAS2-CT-92-0034).

REFERENCES

Berge, P., Y. Pomeau and C. Vidal. 1986. Order within chaos: towards a deterministic approach to turbulence. Wiley, 329+xv pp.

Bryan, F. 1986. High latitude salinity effects and interhemispheric thermohaline circulations. Nature, *323,* 301–304.

Bryan, K. 1969. A numerical method for the study of the circulation of the world ocean. J. Comput. Phys., *4,* 347–376.

Cox, M. 1984. A primitive equation, three dimensional model of the ocean. GFDL Ocean Group Tech. Rep. No. 1.

Lindzen, R. S. 1974. Wave-CISK in the tropics. J. Atmos. Sci., *31,* 156–179.

Marotzke, J. 1991. Influence of convective adjustment on the stability of the thermohaline circulation. J. Phys. Oceanogr., *21,* 903–907.

Numaguti, A. and Y. Hayashi. 1991. Behavior of cumulus activity and the structures of circulations in an "Aqua-Planet" model. Part I: The structure of the super clusters. J. Meteor. Soc. Japan, *69,* 541–561.

Rahmstorf, S. and J. Willebrand. 1995. The role of temperature feedbacks in stabilizing the thermohaline circulation. J Phys. Oceanogr., *25,* 787–805.

Stommel, H. 1961. Thermohaline convection with two stable regimes of flow. Tellus, *13,* 224–230.

Welander, P. 1982. A simple heat-salt oscillator. Dyn. Atmos. Oceans, *6,* 233–242.

Yin, F. L. and E. S. Sarachik. 1994. An efficient convective adjustment scheme for ocean general circulation models. J. Phys. Oceanogr., *24,* 1425–1430.

Received: *5 September, 1995;* revised: *4 January, 1996.*